Critical behavior of the binary fluids cyclohexane-methanol, deuterated cyclohexane-methanol and of their isodensity mixture: Application to microgravity simulations and wetting phenomena

C. Houessou, P. Guenoun, R. Gastaud, F. Perrot, and D. Beysens*
Service de Physique du Solide et de Résonance Magnétique, Commissariat à l'Energie Atomique, Centre d'Etudes Nucléaires de Saclay, F-91191 Gif-sur-Yvette (Cédex), France
(Received 31 January 1985)

It is possible to adjust the density of cyclohexane by adding a small amount of deuterated cyclohexane. Then the mixture deuterated cyclohexane-cyclohexane-methanol can be made isopycnic. We have determined the critical properties of this system and of the systems cyclohexane-methanol and deuterated cyclohexane-methanol: coexistence curve, correlation length, and osmotic compressibility via refractive index and turbidity measurements. For that purpose, a detailed discussion of the validity of the volume additivity and of the Lorentz-Lorenz formula has been made. The main result is that the isopycnic system acts as a binary mixture for the phase transition properties as shown by the β exponent and the amplitude combinations ($R_\xi^+ R_c^{-1/3}$) which exhibit the universal values. Some aspects of microgravity conditions can then be created. We have studied in the isopycnic system the phase separation at critical concentration; new features are found after a thermal quench: macroscopic spinodal decomposition structures during the phase separation process and macroscopic wetting layers in the final equilibrium state.

I. INTRODUCTION

This study is a preliminary step in the investigation of phenomena encountered in fluids submitted to microgravity (MG) conditions, as they appear in space. It also pertains to the first part of a study of wetting phenomena and phase decomposition of fluids—including liquid metals—in a real or simulated low gravity environment.[1]

Since the earth's gravitational acceleration g affects the fluids through the density ρ in the product ρg, the basic idea was to create a mixture where the density of each phase could be adjusted to become as close as possible to each other. For that purpose we initially considered a mixture with components whose densities were nearly matched, the cyclohexane-methanol system (C-M). Adding a small amount of deuterated cyclohexane (C') allows, in principle, the density of the $C+C'$ phase to be adjusted to the M density. The density values are indeed in the range

$$\rho_C < \rho_M \ll \rho_{C'} ,$$

enabling the equality $\rho_{C+C'}=\rho_M$ to be fulfilled. A simple calculation shows that a C'-to-($C+C'$) mass fraction (called c' in the following) of 12.8% should fit this requirement. We will see also that it is rather a concentration $c'=4.5\%$ which makes the system isopycnic in the critical region.

In order to maintain this density matching over a wide range of temperature the thermal expansion coefficients $\alpha=\rho^{-1}(\partial\rho/\partial T)_p$ of the liquid phases should be as close as possible. This condition is fortunately fulfilled by the C, C', and M components.

However, strictly speaking, the ($C+C'$)-M system is a ternary mixture, and it is necessary to determine to what extent it could be assimilated to a real binary fluid. Experiments performed at the mass fraction $c'=11.6\%$ show that the phase-transition properties are the same as if the $C+C'$ mixture acted as a single component. Valuable MG experimental simulations can therefore be performed in such a system, and we will see that new phenomena, such as macroscopic spinodal decomposition patterns and macroscopic wetting layers, can be observed.

This paper is organized as follows: Section II shows physical properties of the C, C', and M components. Section III shows the coexistence curve of the C-M, C'-M, and ($C+C'$)-M (with $c'=11.6\%$) mixtures by refractive index measurements. Section IV shows the osmotic susceptibility and correlation length of the above mixtures using a light transmission technique. Section V shows the check of the critical behaviors (critical exponents) and of the universal relationships between the critical amplitudes (two-scale-factor universality). Section VI shows the application to the simulation of MG conditions (spinodal decomposition process, wetting phenomena).

II. PHYSICAL PROPERTIES OF THE COMPONENTS

A. Chemical purity

The nature and amount of impurities is important in the C-M system; impurities can induce a significant shift of the critical temperature T_c and of the critical mass fraction c_c. This effect is well known.[2–5] The role of water and acetone is dominant. We used the best commercially available quality for the components without further purification:

(i) Methanol. From Merck: the guaranteed purity is better than 99.5%. The main impurities are ethanol (max. 0.1%), water (max. 0.05%), and acetone (max. 0.01%).

(ii) Cyclohexane. From Eastman Kodak company: It is of spectrograde quality, with less than 0.02% of water.

(iii) Deuterated cyclohexane. From Centre d'Etudes Nucléaires de Saclay (CEA-Saclay): the deuterated fraction is guaranteed to be 99.7%. The water fraction is lower than 0.02% and acetone is not detectable.

B. Density

The densities ρ of the components and their thermal variation $\rho^{-1}(\partial\rho/\partial T)_p$ have been experimentally determined using the same batch as used for the mixtures. Measurements have been performed with a commercial densitometer. The principle is to measure the mechanical resonance frequency of a U-tube filled with the liquid. This apparatus needs to be carefully calibrated with two liquids of different densities; we choose as standards water, with density data from Ref. 6, and one of the components, methanol, with density data from Ref. 7. The sensitivity of such measurements is high and to ensure a final ρ accuracy of 10^{-5} a thermal regulation of the sample to within 10 mK is needed. This was obtained by circulating water from a thermostat (Fig. 1). Temperature was measured close to the U tube in the circulating water by a calibrated thermocouple; the other junction was immersed in freezing water and its temperature was controlled by a quartz thermometer. A final resolution of 3 mK was obtained for the temperature measurements. The results for C, C', and $C+C'$ at $c'=5.5\%$ are shown in Fig. 2. The data for water and methanol are not shown since they have been used for the calibration.

The data have been obtained in the T range 25—50 K where the linear variation

$$\rho=\rho_0\left[1+\frac{1}{\rho_0}\left[\frac{\partial\rho}{\partial T}\right]_p(T-T_0)\right] \tag{1}$$

fits the data well. The temperature T_0 was chosen to be 25 °C. The values of the parameters ρ_0 and $\rho_0^{-1}(\partial\rho/\partial T)_p$ are listed in Table I.

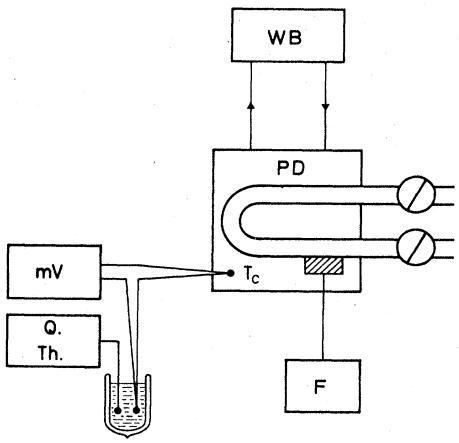

FIG. 1. Setup for measuring the densities of the components. WB, water bath to thermalize the densitometer; PD, densitometer; F, frequency meter; T_C, thermocouple junction; Q. Th., quartz thermometer; mV, millivoltmeter.

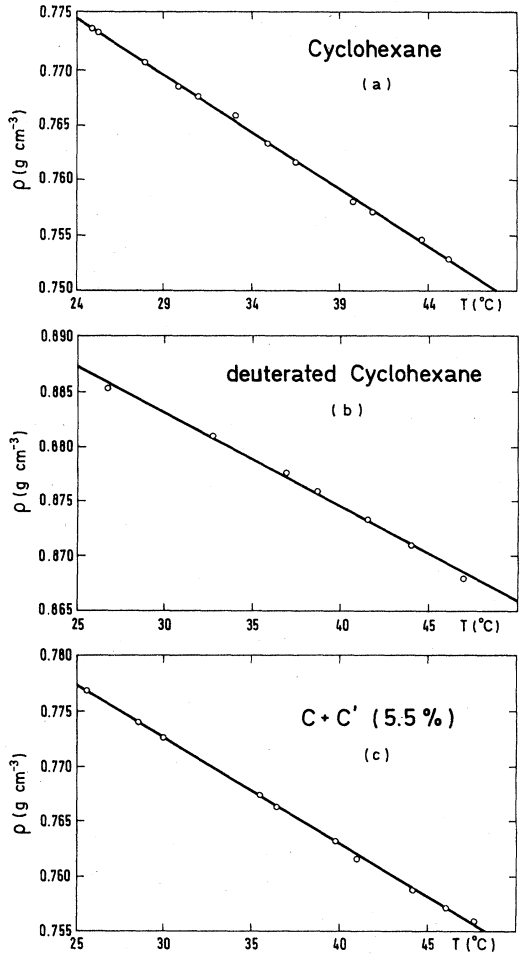

FIG. 2. Density data of cyclohexane (a), deuterated cyclohexane (b), and the mixture of cyclohexane and deuterated cyclohexane at the 5.5% mass fraction of deuterated cyclohexane (c).

Note in Table I that the experimental density of C' is somewhat larger ($=+3\times10^{-3}$) than expected when considering the ratio of the molar weights. Indeed, deuterium exhibits slightly denser electronic orbitals, which makes the liquid somewhat denser than calculated.

We have also compared the $C+C'$ density to that calculated assuming the volume additivity. A discrepancy appears, whose magnitude is about 0.5%. This is small but well above the experimental uncertainty which we estimated to be within 0.1%. Finally a concentration $c'=12.8\%$ should make the density of the $C+C'$ mixture nearly equal to that of methanol.

C. Refractive index

The refractive index measurements have been carried out using the standard method of the "minimum of deviation" (Fig. 3). A high precision parallelepiped shaped cell is filled with the liquid under study. This cell is sealed with a Teflon screwcap. The angle between the windows of the cell has been checked to be $A=90°\pm3'$. This cell is supported by a rotary mount and is immersed in a

TABLE I. Density and refractive index of the components. They have been fitted to the linear variations (1) and (4) in the range 20—50 °C.

Component	ρ_0(25 °C) (g cm^{-3})	$\rho_0^{-1}\left[\frac{\partial\rho}{\partial T}\right]_p$ (K^{-1})	n_0(20 °C, 6328 Å)	$\left[\frac{\partial n}{\partial T}\right]_p$ (K^{-1})
			1.423 50	-5.500×10^{-4}
C	$0.773\,54_2$	$-1.27_7\times10^{-3}$	1.42 356[d]	(-5.561×10^{-4})[d]
			(1.4245)[e]	
C'	$0.887\,17_3$	$-0.95_8\times10^{-3}$		
(99.7%)	$0.884\,24_0$[a]		1.419 43	-5.506×10^{-4}
$C+C'$	$0.777\,32_9$	$-1.23_6\times10^{-3}$		
(5.5%)	$0.779\,03_0$[b]			
$C+C'$	$0.781\,52_9$[c]			
(11.6%)	$0.785\,20_8$[b]			
M	$0.786\,47_7$	$-1.20_7\times10^{-3}$	1.327 11	-4.045×10^{-4}
			1.327 00[d]	(-3.941×10^{-4})[d]
			(1.3274)[e]	

[a]From the C density assuming that the molar density $\rho/\mathcal{M}$ remains constant.
[b]From the C and C' densities assuming the volume additivity.
[c]From the linear extrapolation of the 5.5% ($C+C'$) experimental values.
[d]Imposing the slope $(\partial n/\partial T)_p$ measured in Ref. 10 by interferometric means.
[e]From Ref. 9.

thermally stabilized water bath with accuracy 2 mK. A slightly focused laser beam is sent through the cell. By rotating the cell the minimum of deviation of the beam can be determined, and using a straightforward geometrical calculation one can deduce the corresponding deviation angle D_m.

The refractive index n is a function of A, D_m, and of the refractive index of water n_W:

$$n = n_W \frac{\sin[(A+D_m)/2]}{\sin(A/2)} . \tag{2}$$

In order to use an analytical function for n_W, we have fitted the n_W data of Ref. 8, extrapolated at 6328 Å by using the Ref. 9 data. In the range $T=14$—100 °C, the following formula was found to hold:

$$\begin{aligned} n_W = {} & 1.331\,904 - 9.083\,295\times10^{-5}(T-T_0) \\ & [\,1+1.498\,64\times10^{-2}(T-T_0) \\ & -2.479\,132\times10^{-5}(T-T_0)^2] \end{aligned} \tag{3}$$

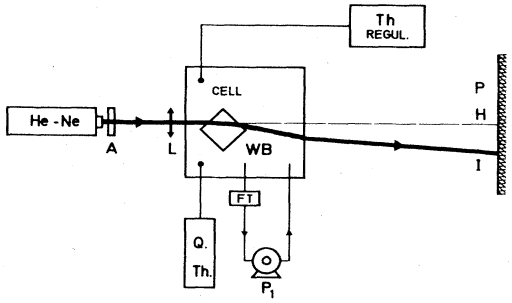

FIG. 3. Experimental setup for refractive index measurements. L, lens; He-Ne, helium-neon laser; A, attenuator; P_1, pump; FT, 8-μm water filter; Q. Th., quartz thermometer; Th. regul., thermal regulation; WB, water bath; P, plane where the beam deviation HI is measured.

with $T_0=18.0859$ °C.

A check of the calibration has been performed by comparing the refractive index of cyclohexane and methanol with literature data[9] extrapolated at the same temperature and wavelength. The remaining discrepancies of a few 10^{-4} are of the order of magnitude of the scatter of data reported by different authors. This scatter can be attributed in particular to the different levels of purity of the components. Another check was performed with silica by sending the beam in the bottom of the cell.

To conclude, we have estimated the absolute accuracy on n measurements to be about 2×10^{-4}; the relative accuracy is larger, it is nearly 5×10^{-5}.

All results concerning the M, C, and C' components and the $C+C'$ mixtures are listed in Table I. In the range investigated ($T=20$—50 °C) the following linear variation is sufficient to fit the data:

$$n = n_0 + \left[\frac{\partial n}{\partial T}\right]_p (T-T_0) . \tag{4}$$

The present work is in good agreement with a previous study of the C and M refractive index by interferometry,[10] where very accurate values for the slope $(\partial n/\partial T)_p$ have been determined. We have imposed these slopes when fitting the data (Table I).

Note the weak lowering ($=-4\times10^{-3}$) of the C' refractive index when compared to the C index. Since C' exhibits a density larger than the C density this result may seem paradoxical. However, let us consider the Lorentz-Lorenz (LL) formula which connects the refractive index to the polarizability a and to the number density per unit volume $\rho/\mathcal{M}$ ($\mathcal{M}$ is the molar weight):

$$\frac{n^2-1}{n^2+2} = \frac{4\pi}{3} a \frac{\rho}{\mathcal{M}} . \tag{5}$$

On deuteration the ratio $\rho/\mathcal{M}$ increases by 0.3% (see Table I); the lowering of n shows that the polarizability of

C' is weaker than that of C. This is in agreement with the lowering of the electronic orbitals, as noted above in Sec. II B for the density.

III. THE COEXISTENCE CURVES

The coexistence curves have been determined, as in Ref. 11 for the C-M mixture, by measuring the refractive index of both phases in the inhomogeneous region. From the refractive index the volume fraction or the mass fraction can be deduced, using some assumptions which will be discussed below.

A. Theory of the measurements

Let us denote by n_u (n_l) the upper (lower) phase. The refractive index can be expressed through the LL formula, known to be valid to within a few percent (Refs. 10 and 11):

$$K_{u\,(l)}=\frac{n^2_{u\,(l)}-1}{n^2_{u\,(l)}+2}=\frac{4\pi}{3}(a_1N_1+a_2N_2)\ . \tag{6}$$

The quantities a_1 (a_2) are the polarizabilities of components 1 (2), and N_1 (N_2) are the number of molecules per unit of volume. We denote here the volume fraction of component 1 in the upper (lower) phase by $\phi^1_{u\,(l)}$ and the corresponding volume fraction of component 2, $\phi^2_{u\,(l)}$. Then (6) can be written,

$$K_{u\,(l)}=K_1\phi^1_{u\,(l)}+K_2\phi^2_{u\,(l)}\ . \tag{7}$$

Here $K_i=(n_i^2-1)/(n_i^2+2)$, with $i=1$ or 2.

The next step needs the assumption of volume additivity. In the C-M system this has been verified to within a few percent by density measurements:[12]

$$\phi^1_{u\,(l)}+\phi^2_{u\,(l)}=1\ . \tag{8}$$

From Eq. (7) it follows

$$\phi^1_{u\,(l)}=(K_{u\,(l)}-K_2)/(K_1-K_2)\ , \tag{9}$$

enabling the volume fraction of component 1 to be determined.

Note that the mass fraction c corresponding to the volume fraction ϕ can be deduced, without any further hypotheses, using the relation

$$c^{-1}=1+(\rho_2/\rho_1)(\phi^{-1}-1)\ . \tag{10}$$

The thermal variation of ρ_1/ρ_2 has to be accounted for. The two assumptions, LL formula and volume additivity, will be checked in the following for the C-M system.

B. Fit of the coexistence curves

We will now consider only the component 1 = cyclohexane and the superscript 1 will be omitted in the following. With T the absolute temperature, and T_c the critical temperature, we will write the reduced temperature as $t=|1-T/T_c|$. The volume fraction or the mass fraction is often considered as the order parameter of the liquid-liquid transition; it is known[13] to follow a universal behavior versus t,

$$\phi_{u\,(l)}=\phi_c\pm B_\phi t^\beta(1+a_\phi t^\Delta)+F_\phi t+G_\phi t^{1-\alpha}+H_\phi t^{2\beta}+\cdots\ . \tag{11}$$

The sign $\pm$ corresponds to the phases (u) or (l). The fraction ϕ_c is the critical volume fraction, B_ϕ is the coexistence curve amplitude, a_ϕ is the first order correction-to-scaling amplitude. F_ϕ, G_ϕ, and H_ϕ are also nonuniversal amplitudes. The exponents are universal:[14] $\beta=0.325$, $\Delta=0.50$, and $\alpha=0.11$.

Generally the accuracy is not good enough to distinguish between the behaviors t, $t^{1-\alpha}=t^{0.89}$, $t^{2\beta}=t^{0.65}$. Therefore we will introduce an "effective" exponent ω with amplitude E_ϕ, whose range will be $\omega=[0.5,1]$. Then Eq. (11) can be rewritten,

$$\phi_{u\,(l)}=\phi_c\pm B_\phi t^\beta(1+a_\phi t^\Delta)+E_\phi t^\omega+\cdots\ . \tag{12}$$

It is sometimes easier to fit the data with the two equivalent expressions,

$$\tfrac{1}{2}(\phi_u-\phi_l)=B_\phi t^\beta(1+a_\phi t^\Delta)\ , \tag{13}$$

$$\tfrac{1}{2}(\phi_u+\phi_l)=\phi_c+E_\phi t^\omega\ . \tag{14}$$

The variations of the mass fraction c vs t can be written in a quite similar manner, with the critical mass fraction c_c, and the amplitudes B_c, a_c, and E_c,

$$c_{u\,(l)}=c_c\pm B_c t^\beta(1+a_c t^\Delta)+E_c t^\omega \tag{15}$$

which can be written as

$$\tfrac{1}{2}(c_u-c_l)=B_c t^\beta(1+a_c t^\Delta)\ , \tag{16}$$

$$\tfrac{1}{2}(c_u+c_l)=c_c+E_c t^\omega\ . \tag{17}$$

C. Experimental

We have used the setup previously described in Sec. II C. The mass fraction of the mixture has been determined by weighing with a resolution of 0.1 mg. Some care was taken to avoid moisture and dust in the final sample, namely, baking the syringes and the cells overnight under vacuum and preparing the mixtures in a dust-free area. Three samples have been prepared at the following concentrations:

C-M, at the C-mass fraction $c_{\text{expt}}=0.7103$;

C'-M, at the C'-mass fraction $c_{\text{expt}}=0.7410$;

$(C+C')$-M, at the concentration $c'=0.116$ and at the $C+C'$ mass fraction $c_{\text{expt}}=0.7100$.

The temperature was lowered by steps. The critical temperature T_c was determined by the appearance of a ring of spinodal decomposition in the scattered light after a thermal quench of a few mK (see Sec. VI A).

The final states of phase separation have been estimated by the disappearance of the droplets and inhomogeneities, i.e., when the fluid becomes transparent. Close to T_c, within a range of some 50 mK, the equilibrium times are very long[15] and can reach 24 hours. These times increase with the density matching of the components, and are therefore maximum for the $(C+C')$-M mixture. However, the density matching of this system at $c'=0.116$ is not as good as calculated, so the equilibrium times remained

in a range comparable to those commonly found in other mixtures. In this last system the denser phase was that of $C+C'$, which indicated that the density matching would have occurred for a smaller c' value. We will see below that this value is nearly $c'=4.5\%$.

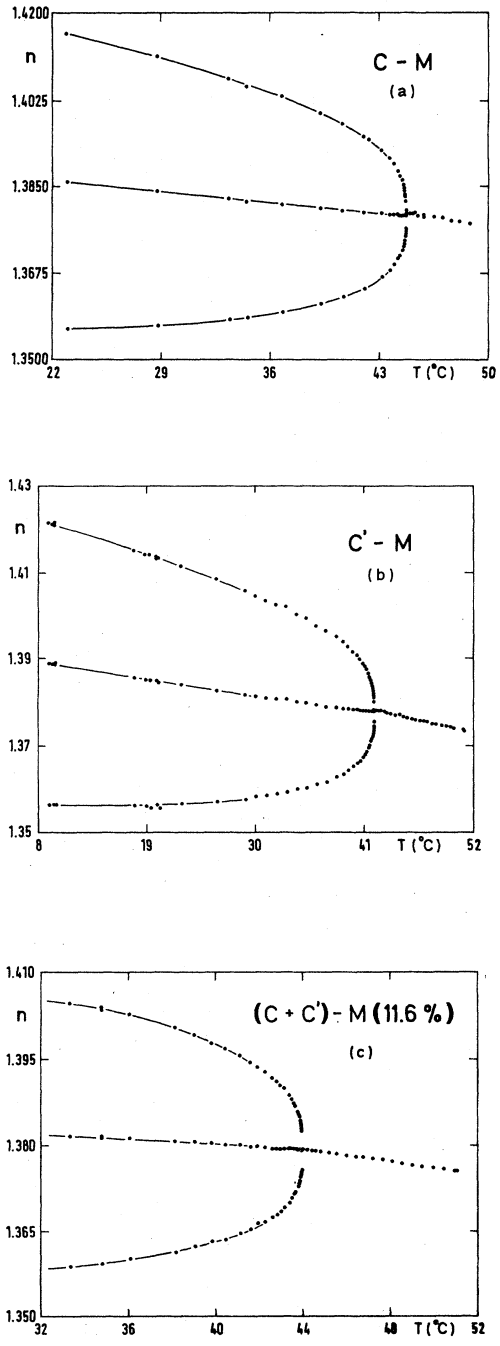

FIG. 4. Refractive index data of the cyclohexane-methanol mixture (a), deuterated cyclohexane-methanol mixture (b) and of the 11.6% mixture of the cyclohexane and deuterated cyclohexane-methanol system (c). Both the one-phase and the two-phase regions have been investigated.

D. Results

The refractive index variations are drawn in Fig. 4. The measurements have been performed in both the one-phase and two-phase regions.

1. Direct analysis of the refractive index

(i) In the homogeneous region $T>T_c$ the refractive index is expected to behave as

$$n=n^+_{\text{expt}}+T_c\left[\frac{\partial n}{\partial T}\right]_{p,\phi}t+Rt^{1-\alpha}\,. \tag{18}$$

Here n^+_{expt}, $(\partial n/\partial T)_{p,\phi}$, and R are nonuniversal amplitudes. The $t^{1-\alpha}$ behavior is related to the density anomaly, whose amplitude is small in this system.[12] Since the exponent α is small (0.11), the uncertainty of our measurements allows the following simplification to be made:

$$n=n^+_{\text{expt}}+At\,. \tag{19}$$

The data fit well this simple linear variation where n^+_{expt} and A are the adjustable parameters. Results are reported in Table II.

(ii) In the inhomogeneous region $T<T_c$ we will simply apply the order parameter behavior [Eq. (12)] to the refractive index. Indeed the refractive index variations are relatively small and the coupling parameter $(\partial n/\partial\phi)$ remains nearly constant in the T range investigated, as already noticed in Ref. 11. The refractive index is therefore expected to exhibit the behavior

$$n=n_c\pm B_n t^{\beta}(1+a_n t^{\Delta})+E_n t^{\omega}\,. \tag{20}$$

Note that this expression is somewhat approximate since a number of approximations which are not well controlled have been performed. We will discuss this point later.

Instead of Eq. (20) we fitted the data with the two equivalent expressions,

$$\tfrac{1}{2}(n_u-n_l)=B_n t^{\beta}(1+a_n t^{\Delta})\,, \tag{21}$$

$$\tfrac{1}{2}(n_u+n_l)=n_c+E_n t^{\omega}\,. \tag{22}$$

The parameters n_c, B_n, a_n, and E_n are adjustable. The exponent β has either been set free or imposed at the theoretical value 0.325. The exponent ω was imposed to be equal to unity. The exponent Δ was imposed to the value 0.5. In fact we were unable to detect corrections to scaling, and the results reported in Table II were obtained with a_n set to zero. This result is in agreement with the study of the C-M system of Ref. 10.

The Table II results deserve some comments:

(a) The values of n^+_{expt} and n_c do not coincide, as is obvious from Fig. 4. This means that the mixtures were not prepared at the exact critical concentration.

(b) The critical exponent β is found to be not too far from the theory, especially for the $(C+C')$-M mixture.

(c) The comparison with already published data for the C-M system shows a remarkable agreement, except for the β value that we have found to be slightly larger.

In order to compare the amplitudes of the coexistence curves of the different mixtures we need to analyze the

TABLE II. Refractive index fitted to Eq. (19) when $T > T_c$ and Eqs. (21) and (22) when $T < T_c$. The values in parentheses have been imposed in the fits. Corrections-to-scaling terms have been found negligible.

		$T > T_c$			$T < T_c$			
					n_c	B_n	E_n	β
System	c_{expt}	n^+_{expt}	$\left[\frac{\partial n}{\partial T}\right]_{p,\phi}$ (K^{-1})	T_c (°C)	(β=0.325,ω=1)	(β=0.325)	(ω=1)	(all free)
C-M	0.710_3	$1.379\,79_4$	-5.08×10^{-4}	44.826	1.379 19	0.071 35	9.7×10^{-2}	0.334
					±0.000 30	±0.000 40	$\pm1.4\times10^{-2}$	±0.004
	0.710_6[a]	1.379 66[a]	-5.82×10^{-4}	45.474[a]	1.379 56[a]	0.071 5[a]	9.43×10^{-2a}	0.326[a]
								±0.003
C'-M	0.741_0	$1.378\,37_9$	-5.40×10^{-4}	42.130	1.377 45	0.065 52	9.96×10^{-2}	0.337
					±0.000 20	±0.000 30	$\pm0.5\times10^{-2}$	±0.002
C+C'-M (11.6%)	0.710_0	$1.379\,45_7$	-5.50×10^{-4}	44.034	1.379 38	0.070 57	7.27×10^{-2}	0.322
					±0.000 02	±0.000 35	$\pm0.17\times10^{-2}$	±0.002

[a]From Ref. 10.

TABLE III. Determination of the *C-M* coexistence curve parameters. The data of different origins have been fitted to Eq. (15) (sets a and b) or Eq. (16) (from refractive index). The order parameter is the *C*-mass fraction. The values in parentheses have been imposed in the fit.

	T_c	c_c	B_c	a_c	E_c	ω	β	χ^2
From	45.1417	0.715	0.738	−0.087	−0.36	0.65	(0.325)	14.7
Eckfeldt	±0.0013	±0.003	±0.02	±0.13	±0.13	±0.12		
and	45.1417	0.715	0.718	(0)	−0.36	0.64	0.321	15.0
Lucasse[a]	±0.0013	±0.003	±0.02		±0.13	±0.12	±0.007	
	45.1419	0.715	0.727	(0)	−0.36	(0.65)	(0.325)	15.5
	±0.0013	±0.002	±0.005		±0.02			
	45.1424	0.711	0.725	(0)	−1.05	(1)	(0.325)	26.2
	±0.0016	±0.002	±0.005		±0.06			
From	45.600[c]	0.720[c]	0.781	−0.29	−0.50	0.77	(0.325)	186
Jones	±0.001	±0.004	±0.03	±0.15	±0.20	±0.15		
and	45.600[c]	0.720	0.711	(0)	−0.6	0.83	0.316	212
Amstell[b]	±0.001	±0.004	±0.03		±0.2	±0.16	±0.013	
	45.600[c]	0.720	0.788	−0.33	−0.36	(0.65)	(0.325)	196
	±0.001	±0.004	±0.03	±0.15	±0.03			
	45.600[c]	0.720	0.729	(0)	−0.37	(0.65)	(0.325)	244
	±0.001	±0.004	±0.01		±0.03			
	45.600[c]	0.720[c]	0.770	−0.22	−0.89	(1)	(0.325)	209
	±0.001	±0.004	±0.03	±0.15	±0.07			
	45.600[c]	0.720	0.732	(0)	−0.915	(1)	(0.325)	229
	±0.001	±0.004	±0.01		±0.08			
From	(44.826)		0.768	−0.085			(0.325)	47
our			±0.006	±0.05				
refractive	(44.826)		0.752	(0)			0.323	51
index			±0.010				±0.003	
data	(44.826)		0.759	(0)			(0.325)	52
			±0.003					
	(44.826)	0.6738			−0.34	0.76	(0.325)	29
		±0.0004			±0.04	±0.04		
	(44.826)	0.6749			−0.245	(0.65)	(0.325)	40
		±0.0004			±0.006			
	(44.826)	0.6722			−0.67	(1)	(0.325)	70
		±0.0004			±0.02			

[a]Reference 3.
[b]Reference 2.
[c]The fitting program could not give the uncertainties due to some problems created by an imposed range for T_c and c_c. We have estimated the errors.

TABLE IV. Comparison between the C-M parameters when using the C-mass fraction as an order parameter. The C-mass fraction has been obtained: (a) from the direct measurements of Ref. 3 and Table III, (b) from the direct measurements of Ref. 2 and Table III, (c) from our refractive index measurements (see Table III), assuming both the L-L formula and the volume additivity, and (d) corrected from these above (c) assumptions (see text and Table VI). The quantity δ is the correction between the direct measurements $[Y(c)]$ and the refractive index ones $[Y(n)]$, such as $Y(c)=Y(n)(1+\delta)$.

Parameter Y	Eckfeldt and Lucasse (a)	Jones and Amstell (b)	Average of (a) and (b)	From (n) (c)	δ (%)
T_c (°C)	45.142	45.600	45.371	44.826	
c_c	0.715	0.720	0.717_5	0.675	6.30
$(\omega=1)$				0.704[d]	1.92[d]
B_c	0.727	0.729	0.728	0.759	4.25
$(\beta=0.325, a_m=0)$					
E	−1.05	−0.91	−0.98	−0.67	−46
$(\omega=1)$					
β	0.321	0.316		0.323	
$(a_m=0)$	±0.007	±0.013		±0.003	
ω	0.65	0.77		0.76	
	±0.12	±0.15		±0.04	

volume (or mass) fraction variations. Before that we will check in the C-M mixture the assumptions of Sec. III B which allows the connection n-ϕ or n-c to be made.

2. *Comparison of the C-M coexistence curves using refractive index or direct measurements*

The LL formula and the volume additivity have been checked as follows. We have fitted the coexistence curves of Refs. 1 and 2, where the mass fraction was directly determined, to the behavior (15). We have imposed in the fits the exponents β and Δ at their theoretical value 0.325 and 0.5. The exponent ω, as the amplitudes c_c, B_c, a_c, and E_c, were left free. The results can be found in Table III. The values inferred from the two studies are in excellent agreement.

We have also applied Eqs. (9) and (10) to the refractive index data in order to infer the mass fraction, which has been fitted to the behaviors (16) and (17). The results are shown in Table III and can be compared to the direct measurements (for the comparison, Table IV is helpful):

(i) The values obtained for the exponents β and ω are in good agreement and very close to the theoretical values $\beta=0.325$ and $\omega=2\beta=0.65$.

(ii) The amplitudes exhibit some differences. In Table IV we have made visible the relative deviation δ of an amplitude obtained from n, i.e., $Y(n)$, or directly from c, i.e., $Y(c)$. The deviation δ is defined as

$$\delta=[Y(c)-Y(n)]/Y(n) .$$

This deviation remains small for both B_c and c_c, but reaches nearly 50% for E.

Nevertheless we can reasonably expect that these deviations will remain almost constant when comparing the different mixtures, and that valuable relative comparisons will be possible.

3. *Analysis of the C-M, C′-M, and (C+C′)-M coexistence curves*

We have applied Eqs. (9) to analyze the volume fraction, using the behaviors (13) and (14). The amplitudes ϕ_c, B_ϕ, and E_ϕ were left free, and the exponent β was either left free or imposed. The exponent ω was set equal to unity.

The results of the fits are reported in Table V. It is clear that when cyclohexane is deuterated, not only T_c changes, but so do also all the amplitudes. The relative

TABLE V. Coexistence curves fitted to Eqs. (13) and (14) with the volume fraction ϕ as an order parameter. Both the LL formula and the volume additivity have been assumed. The values in parentheses have been imposed in the fits.

System	T_c (°C)	ϕ_c $(\omega=1,\beta=0.325)$	B_ϕ $(\beta=0.325)$	E_ϕ $(\omega=1)$	β
C-M	(44.826)	0.6760±0.005	0.755±0.003	−0.695±0.022	0.323±0.003
C'-M	(42.130)	0.671±0.001	0.713±0.002	−0.642±0.026	0.326±0.002
$(C+C')$-M (11.6%)	(44.034)	0.6775±0.0002	0.752±0.002	−0.968±0.020	0.322±0.002

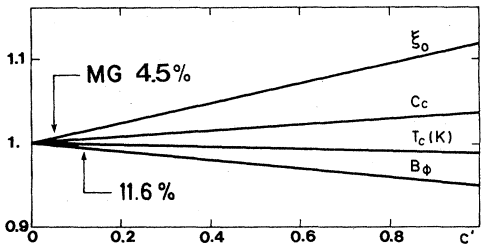

FIG. 5. Variations of some critical amplitudes versus the C'-to-$(C+C')$ mass fraction in the critical mixture $(C+C')$-M. The values are reduced to the C-M system.

change however remains small (see Fig. 5). Note that the values found for the exponent β in Table V are very close to the theory 0.325.

4. *Corrections to obtain the critical mass fraction*

From a practical point of view, it is important to infer from these measurements the critical mass fraction with the maximum reliability. For that purpose we have developed a correction procedure where the LL and volume additivity assumptions have little effect.

We know the experimental mass fraction c_{expt} of the system under study, and the corresponding refractive index at T_c (n^+_{expt}, from Table II). From the refractive index fit below T_c one deduces the critical index n_c (Table II). Since the difference between n_c and n^+_{expt} is small one can write

$$c_c^c = c_{\text{expt}} + \left[\frac{\partial c}{\partial n}\right](n_c - n^+_{\text{expt}}) \ . \tag{23}$$

Here c_c^c is the corrected critical mass fraction and $(\partial n/\partial c)$ is the slope at (T_c, c_c), derived from Eqs. (9) and (10),

$$\left[\frac{\partial n}{\partial c}\right] \simeq (K_1 - K_2)\frac{(n_c^2+2)^2}{6n_c} \ . \tag{24}$$

The results are listed in Table VI.

It is interesting to compare these estimates with the value found in the volume fraction fit (Table V). For that purpose we have estimated the mass fraction c_c through Eq. (10). The results of Table VI show a constant and systematic deviation of about 3%, which therefore measures the level of accuracy of the assumptions concerning the LL formula and the volume additivity.

IV. OSMOTIC SUSCEPTIBILITY AND CORRELATION LENGTH

We used light scattering techniques—more precisely light transmittance measurements—in order to obtain two basic critical properties, the correlation length and the osmotic compressibility.

A. Theory of the measurements

The large concentration fluctuations which take place near the liquid-liquid critical point of a binary fluid make the refractive index fluctuate in space and time (if the refractive indices of the components are different). The coupling parameter is the derivative $(\partial n/\partial c)_{p,T}$. Light is strongly scattered by the fluid; it is the classical critical opalescence. The light scattering attenuates the incident light. The measurement of the transmittance $\mathcal{T}$ in a sample of length L, or equivalently of the turbidity τ such that

$$\tau = (-1/L)\ln\mathcal{T} \tag{25}$$

allows two properties of the fluctuations to be determined:

(i) The amplitude, related to the turbidity amplitude.

(ii) The size, owing to interference terms which appear because the light wavelength becomes comparable to the fluctuations extent.

A good approximation of the correlation function of the concentration fluctuations is given by the Ornstein-Zernike function,

$$\langle \delta c(0)\delta c(r)\rangle = \left[\frac{\partial c}{\partial \mu}\right]_{p,T} k_B T \frac{e^{-r/\xi}}{r} \ . \tag{26}$$

The variable r is the space coordinate. The parameter ξ is the correlation length of the fluctuations and exhibits a universal behavior near T_c (Ref. 14),

$$\xi = \xi_0 t^{-\nu} \ . \tag{27}$$

The exponent $\nu = 0.63$ is universal, and ξ_0 is a nonuniversal amplitude.

The osmotic compressibility $(\partial c/\partial \mu)_{p,T}$ is the inverse derivative versus c of the chemical potential difference

$$\mu = (\mu_1 - \mu_1^c) - (\mu_2 - \mu_2^c) \ ,$$

TABLE VI. Determination of the corrected critical mass fraction c_c^c by correcting the Lorentz-Lorenz formula and the volume additivity hypotheses (see text).

System	c_{expt}	c_c[a]	n^+_{expt}[b]	n_c[b]	$\left[\frac{dc}{dn}\right]$[c]	$c_c^c - c_c$	c_c^c[a]
C-M	0.7103	0.6722	1.379 794	1.379 19	10.69	3.16×10^{-2}	0.7038
C'-M	0.7410	0.6963	1.378 379	1.377 45	11.12	3.43×10^{-2}	0.7307
$(C+C')$-M	0.7100	0.6775	1.379 457	1.379 38	10.73	3.17×10^{-2}	0.7092

[a]From ϕ_c from Table V and calculating c_c by means of Eq. (10).
[b]From Table II.
[c]From Eq. (24).

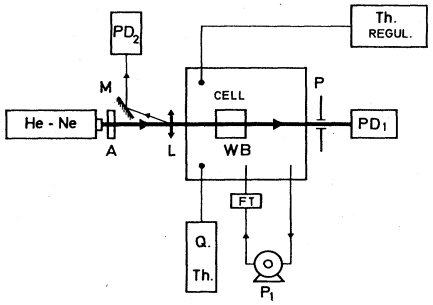

FIG. 6. Experimental setup for measuring the turbidity. L, lens; He-Ne, helium-neon laser; P, pin-hole; A, attenuator; M, mirror; P_1, pump; FT, 8-μm water filter; Q. Th., quartz thermometer; PD_1,PD_2, calibrated photodiodes; Th. regul., thermal regulation; WB, water bath.

where the quantities μ_i ($i=1$ or 2) are the chemical potential of the components, and μ_i^c the value at T_c. The osmotic compressibility exhibits a universal behavior,[14]

$$\left[\frac{\partial c}{\partial \mu}\right]_{p,T} = \frac{C^+}{k_B T_c} t^{-\gamma} . \tag{28}$$

Here $\gamma=1.24$ is a universal exponent and C^+ is a nonuniversal amplitude.

The turbidity τ is related to both ξ and $(\partial c/\partial \mu)_{p,T}$ by the classical expression[16]

$$\tau=\tau_0(1+t)t^{-\gamma}G(X)+\tau_B , \tag{29}$$

where

$$\tau_0=\frac{\pi^3}{\lambda_0^4}S_n^2\left[\frac{\partial n^2}{\partial c}\right]^2 C^+ . \tag{30}$$

Here $(\partial n^2/\partial c)$ is the square of refractive index derivative versus concentration; we will make use as concentration of the volume fraction ϕ in order to be consistent with the coexistence curve study: $(\partial n^2/\partial c)\equiv(\partial n^2/\partial \phi)$.

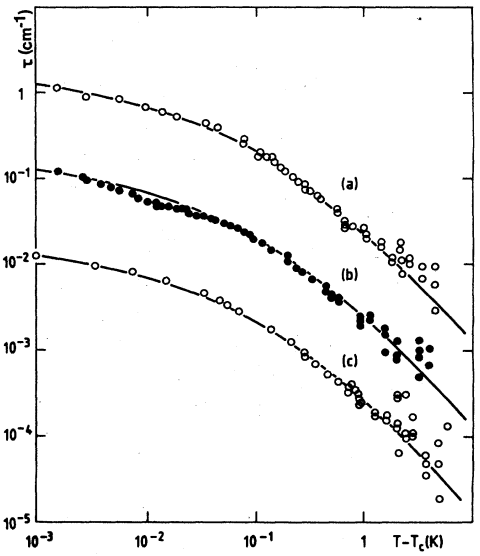

FIG. 7. Turbidity τ as a function of temperature: (a) τ in the cyclohexane-methanol mixture; (b) 0.1τ in the deuterated cyclohexane-methanol mixture; (c) 0.01τ in the 11.6% mixture of cyclohexane-deuterated cyclohexane-methanol system. Note the log-log plot. The line is the best fit to Eq. (29) with the parameters listed in Table VII.

The parameter τ_B represents the noncritical causes of absorption, and the parameter S_n is connected to the local field evaluation, in a way quite similar to the Lorentz-Lorenz formula. We will consider here the formulation proposed by Yvon[17] or Vuks[18] which was seen to hold in the binary fluids[19]

$$S_n=\frac{9n^2}{(n^2+2)(2n^2+1)} . \tag{31}$$

The function $G(X)$ takes into account the interference terms which appear when the correlation length becomes comparable to the light wavelength; with $k=2\pi n\sqrt{2}/\lambda_0$ a typical wavevector and $X=(k\xi)^2$, $G(X)$ can be written[16]

TABLE VII. Determination of the amplitudes C^+ and ξ_0 from turbidity measurements at $\lambda_0=6328$ Å. Data have been fitted to Eq. (29).

System	$(\partial n/\partial\phi)_{p,T}$[a]	n_c[b]	τ_0 (10^{-6} cm^{-1})	τ_B (10^{-3} cm^{-1})	C^+ (10^{-23} cm^3)	ξ_0 (Å)
C-M	9.423×10^{-2}	1.379 19	6.74±0.53	4.5±4.5	6.19±0.5	3.24±0.23
C'-M	9.321×10^{-2}	1.377 45	5.91±0.65	6.5±7	5.55±0.6	3.60±0.30
C+C'-M	8.563×10^{-2}	1.379 38	7.14±0.30	7.5±3	7.94±0.35	3.30±0.12

2.40[c]
4.1±0.5[d]
3.9±1[e]
3.5±0.4[e]

[a]From the derivative of Eq. (9).
[b]From Table II.
[c]From Ref. 29.
[d]From Ref. 30.
[e]Values obtained indirectly from the specific heat data of Ref. 31 analyzed in Ref. 20.

TABLE VIII. Comparison of the universal exponent β and of the universal combination $\xi_0(B_\phi^2/C^+)^{1/3}$ in the different mixtures.

System	β[a] (0.325 theory)	B_ϕ[a]	ξ_0[b] (10^{-8} cm)	C^+[b] (10^{-23} cm^3)	$\xi_0(B_\phi^2/C^+)^{1/3}$ (0.67 theory)
C-M	0.323±0.003	0.755±0.003	3.24±0.23	6.19±0.5	0.68±0.07
C'-M	0.326±0.002	0.713±0.002	3.60±0.30	5.55±0.6	0.75±0.09
$(C+C')$-M (11.6%)	0.322±0.002	0.752±0.002	3.30±0.12	7.94±0.35[c]	0.64±0.04[c]

[a]From Table V.
[b]From Table VII.
[c]This value is slightly different from the one reported in Ref. 1 due to a reanalysis of the data.

$$G(X)=\frac{2X^2+2X+1}{X^3}\ln(1+2X)-\frac{2(1+X)}{X^2}\ . \tag{32}$$

The asymptotic limits of $G(X)$ are

$$X\ll 1,\quad G(X)\propto \tfrac{8}{3},\quad \text{and}\quad \tau\propto t^{-\gamma}\ , \tag{33a}$$

$$X\gg 1,\quad G(X)\propto \frac{\ln X}{X},\quad \text{and}\quad \tau\propto \ln t\ . \tag{33b}$$

In the region far from T_c where G is a constant, the amplitude C^+ can be determined, and close to T_c it is the amplitude ξ_0 which can be measured. A simple set of turbidity measurements allows, in principle, these amplitudes to be obtained.

Note that the only remaining difficulty concerns the determination of C^+ which is a function of the choice of S_n. Although we think that the Yvon formulation is the more correct, this problem affects only the absolute value of C^+, and not the comparison between values obtained from the different mixtures of C, C', and M.

The same remark can be made about the correlation length whose value can be different according to the different correlation functions which have been assumed. More accurate correlation functions have been proposed,[14] which generally lead to very small differences in G.

B. Experimental

The setup (Fig. 6) is nearly the same as that of (Fig. 3) used for the refractive index measurements. The cell, whose inner path is 1.000±0.001 cm, is also the same. The laser beam was sent perpendicularly to the entrance window. The light power was reduced to less than 1 mW in order to reduce extra heating of the sample (typically 0.5 mK per mW incident power). The transmitted beam was detected by a calibrated photodiode after having passed through a pinhole; this reduced the scattered and multi- scattered light contributions to a level where they remained negligible. The cell was moved upwards in order to measure the incident beam intensity. The laser intensity was detected by another calibrated photodiode. Several runs in temperature have been performed.

C. Results

The turbidity data concerning the three mixtures are reported in Fig. 7. They have been fitted to Eq. (29) where only the parameters C^+, ξ_0, and τ_0 were left free. Our experimental procedure allows τ_B to be identified with the reflection losses of the cell,

$$\tau_B=\frac{2}{L}\left[\left[\frac{n_S-n_W}{n_S+n_W}\right]^2+\left[\frac{n_S-n_c}{n_S+n_c}\right]^2\right]\simeq 4\times 10^{-3}\ \text{cm}^{-1}\ , \tag{34}$$

where n_S is the silica refractive index.

In Table VII are reported the values of the above parameters measured in the three mixtures. One can see that their variation according to the different systems remains small.

TABLE IX. Values of some parameters interpolated at the C'-mass fraction of 4.5%, for which the mixture $(C+C')$-M is isopycnic.

T_c (°C)	c_c (mass fraction)	B_ϕ	ξ_0 (Å)	$C^+(10^{-23}$ cm$^3)$
44.48	0.7061	0.7540	3.265	7.02

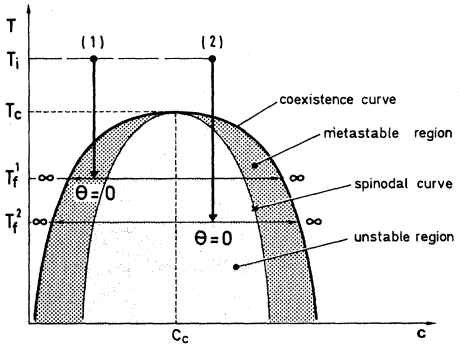

FIG. 8. Phase separation of a binary fluid. At time $\theta=0$ the system is quenched from the temperature T_i in the one-phase region to T_f under the coexistence curve. It then phase separates to reach the coexistence curve at the end of the process ($\theta\to\infty$). The hatched region under the coexistence curve is not stable. The spinodal curve classically separates a region of metastability where nucleation occurs in the phase separation process [labeled (1)] from a region of unstability where spinodal decomposition takes place [labeled (2)].

A comparison with other determinations[20] can be made for the C-M system. Our result $\xi_0=3.24\pm0.23$ Å agrees well with the most recent determinations of Ref. 20, $\xi_0=3.9\pm1$ Å and $\xi_0=3.5\pm0.4$ Å.

V. UNIVERSAL BEHAVIORS

Checks of the critical universal behaviors have been made on the following points.

A. Value of critical exponents

The fit of the turbidity data of the $(C+C')$-M system by Eq. (29) means that the correlation length and the susceptibility behave in this system as in normal binary fluids. A more sensitive test lies in the comparison of the critical exponents β as determined in Sec. III D 3. The values are reported in Table VIII and are in fair agreement, not only with each other but also with the theoretical value 0.325.

B. Universal relationships between the amplitudes

We have determined here three amplitudes: B_ϕ, C^+, and ξ_0. They are not independent, and the following combination is expected to have a universal value:[19]

$$R_\xi^+(R_c)^{-1/3}=\xi_0\left[\frac{B_\phi^2}{C^+}\right]^{1/3}=0.67 \tag{35}$$

according to the most recent determination using the renormalization group theory.[21,22]

We have reported in Table VIII the above combination for the three mixtures; a good agreement is found with the theoretical value.

C. Concluding remarks

We therefore see that all the tests performed with the C-M, C'-M, and $(C+C')$-M mixtures did not show any ternary character of the $(C+C')$-M system, at least for the phase transition phenomena.

The nonuniversal amplitudes, however, were seen to (slightly) vary with the concentration of C'; in Fig. 5 are drawn the corresponding variations. The isodensity in the critical point vicinity occurs for a C' concentration of 4.5% and the amplitudes of the corresponding mixture is nearly those of the C-M system. In Table IX we have reported the values interpolated at $c'=4.5\%$ for T_c, c_c, B_ϕ, ξ_0, and C^+.

VI. EXPERIMENTAL REPRODUCTION OF A MICROGRAVITY ENVIRONMENT

A simple calculation cited in Sec. II B shows that a mixture of C and C' at the mass fraction $c'=12.8\%$ should exhibit the same density as M. However, this is not experimentally the case when considering a critical mixture $(C+C')$-M.

We have performed systematic experiments by varying c' and by looking at the Laplace length (l) of the meniscus between the 2 phases within a few tens of mK below T_c. The concentration which gave the isodensity corresponded to a Laplace length of the order of the sample size. This is a very sensitive test because of the density and temperature dependence of l:

$$l=\left[\frac{2\sigma}{g\,\Delta\rho}\right]^{1/2}. \tag{36}$$

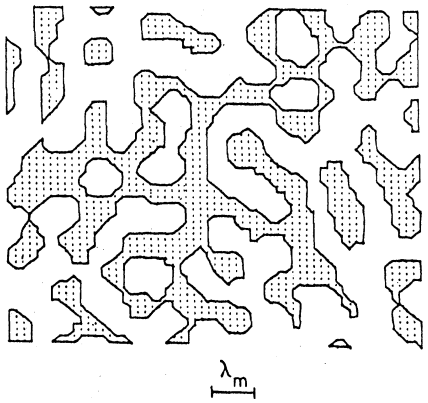

FIG. 9. Computer simulation of a spinodal decomposition structure. λ_m is the typical wavelength. From Ref. 26.

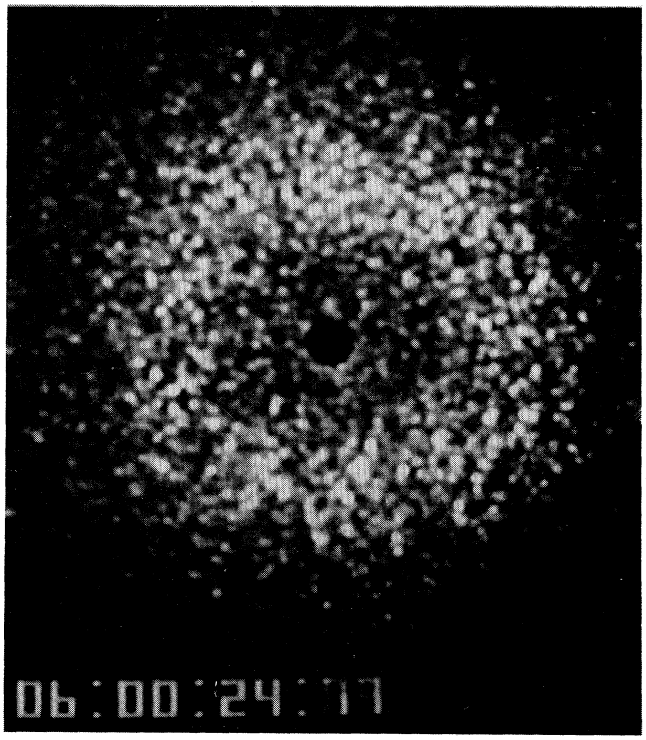

FIG. 10. Typical ring structure of the light scattered by a binary fluid undergoing spinodal decomposition. The corresponding wavelength is $\lambda_m\simeq11$ μm (C'-M mixture, 24.77 sec after a thermal quench at $T_f-T_c=-1$ mK).

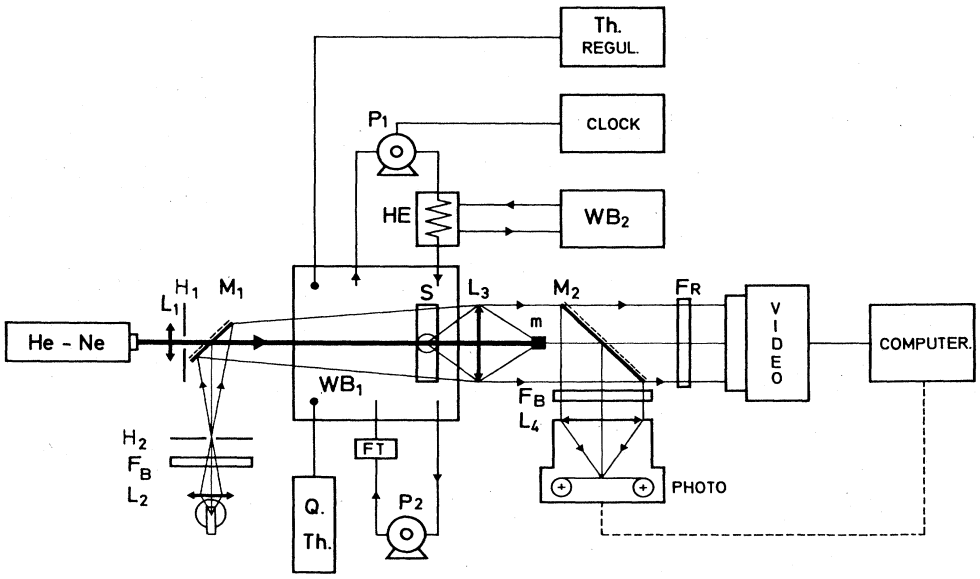

FIG. 11. Experimental setup for studying the phase separation processes. L_1,L_2,L_3,L_4, lenses; He-Ne, helium-neon laser; H_1,H_2, pin-holes; F_B, blue colored filters; F_R, red interferential filter; M_1,M_2, semitransparent mirrors; m, mask; S, sample cell; P_1,P_2, pumps; WB_1,WB_2, temperature regulated water baths; Q. Th., quartz thermometer; Th. regul., thermal regulation; HE; heat exchanger; FT, water filter.

Here σ is the interfacial tension and $\Delta\rho$ the density difference of the two phases. Near T_c, σ exhibits a universal behavior,

$$\sigma=\sigma_0(-t)^{\mu}, \tag{37}$$

where $\mu=2\nu=1.26$ is a universal exponent[23] and σ_0 a nonuniversal amplitude. In the C-M mixture $\sigma_0=114$ dyn/cm (Ref. 24) and a Laplace length of 1 cm at 30 mK from T_c corresponds to a density difference $\Delta\rho=10^{-6}$ g cm^{-3}.

The more the temperature is close to T_c, the more sensitive is the test. Indeed the density difference between the two phases goes to zero as their relative composition, i.e., slower than σ. According to the developments of Sec. III B,

$$\Delta\rho=\Delta\rho_0(-t)^{\beta}, \tag{38}$$

where $\Delta\rho_0$ is an amplitude. This means that l must go to zero when approaching T_c, whatever the level of accuracy of the density matching (or MG),

$$l=\left[\frac{\sigma_0}{g\,\Delta\rho_0}\right]^{1/2}(-t)^{(\mu-\beta)/2}\propto(-t)^{0.47}. \tag{39}$$

A good matching was found for the C'-mass fraction $c'=4.5\pm1\%$. This is less than half the value expected. We attribute this difference to the anomaly of volume additivity which occurs near T_c, and which amounts to a few % in the C-M mixture.[12] The uncertainty is related to the amount of impurities, as these modify the relative density of the two phases. Let us consider for instance water as the impurity, and assume that it mixes only with methanol. A concentration of 0.02% will give rise to a density variation of 10^{-6} g/cm^3 at $T-T_c=-10$ mK. This density variation can be larger than the difference in density between the two pure phases. Because of some uncontrolled parameters during the sample preparation process, the isopycnic mixtures show concentrations of between 3.5% and 5.5% c' mass fraction.

It is likely that the density or volume anomaly is more t dependent than the difference in the volume expansion of the pure components and would cause some density mismatch far from T_c. It is why we have limited here our study to the region $T_c-T=1$ K, and to two phenomena: phase separation process and wetting layers. The corresponding results are only preliminary.

A. Phase separation process: Spinodal decomposition

If a binary fluid is subjected to a thermal quench ($T_i>T_c$ to $T_f<T_c$) from its homogeneous region to its two-phase region, it phase separates (Fig. 8). At the critical concentration the system separates—at least initially—according to a spinodal decomposition (SD) process, to be compared with the phenomenon of nucleation.[25] In the SD process all fluctuations become unstable and grow with time θ. The rate of growth is size dependent, and this favors a typical size or wavelength λ_m for which the rate is maximum, to appear in the system. The wavelength λ_m is itself time dependent; at constant temperature,

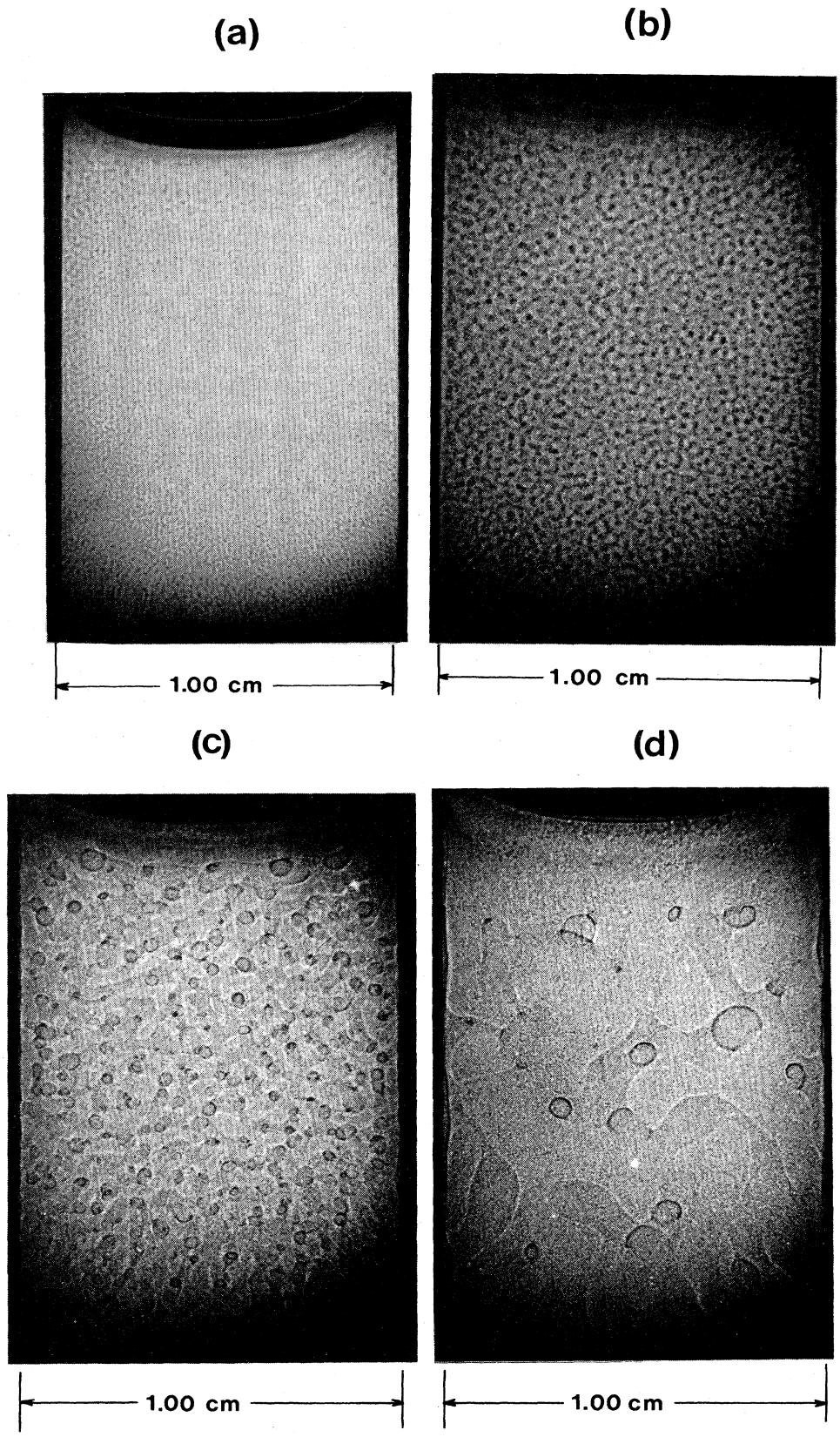

FIG. 12. Aspect of a 1×0.2-cm sample of the isopycnic $(C+C')$-M mixture after a quench of 10 mK below T_c. (a) 1 min 20 sec after the quench. (b) 2 min after the quench. (c) 4 min after the quench. (d) 9 min after the quench.

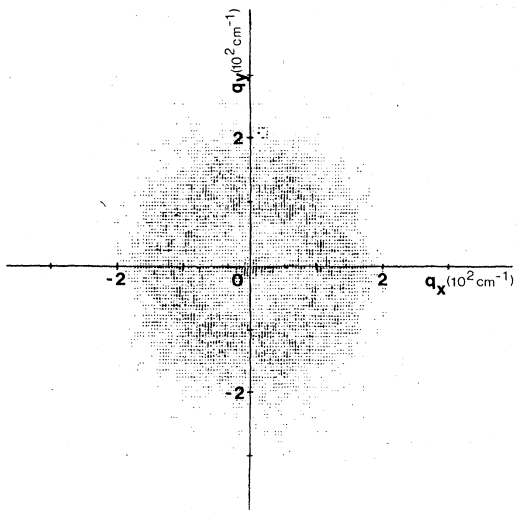

FIG. 13. Fourier transform of Fig. 12(a). We have selected 8 levels (the intensity is proportional to the point density). Compare this ring to that in Fig. 10.

$$\lambda_m \propto \theta^{1/3} \text{ for small } \theta\,, \tag{40}$$

$$\lambda_m \propto \theta \text{ for large } \theta\,. \tag{41}$$

A simulation of the process (Fig. 9) leads to consider the two-dimensional pattern as the sum of phase-aleatory Fourier modes with the same wavelength λ_m (Refs. 26 and 27).

Typically the detectable structures are in the range of a few μm (glasses, metallic alloys, etc.) and can be studied by electron microscopy. Diffraction techniques are also used, such as x-ray or visible light scattering. In these last cases a typical SD ring pattern is observed (Fig. 10), which is the Fourier transform of the SD structure.

In fluids the final stages of the SD process are difficult to observe; before λ_m reaches large values, instabilities (convections) driven by gravity occur, which make the denser phase to go to the bottom of the sample, and the lighter to the top. Making the density difference (or the parameter g) very small would allow these late stages to be observed.

B. Experimental

We carried out an experiment (Fig. 11) in order to observe both the initial SD process ($\lambda_m \simeq 1$ μm) and the final processes ($\lambda_m \simeq 1$ cm). When λ_m does not exceed a few μm, a classical light scattering setup was used. For larger values a Schlieren optics device has been chosen. These two techniques can operate at the same time owing to colored filters which separate the red light ($\lambda = 6328$ Å) of the scattering experiment from the blue light of the Schlieren optics illumination.

The samples used were 2.00 mm thick (light path), 1 cm wide, and 2 cm high. In some cases we have used also cylindrical cells with 2 cm diameter and 2 mm thickness. The cells were sealed by a Teflon screwcap as above. The mixture was made of C and C' at the mass fraction $c' = 4.5\%$, and M, so that the mixture was at the critical mass fraction of 0.706 as reported in Table IX.

The thermostat was the same as before. The thermal quench was accelerated by injecting during a calibrated time water at a given temperature. The total typical time response was 15 sec as measured directly in the sample by light transmittency measurements.

The scattered light and/or the sample image were recorded by a photo camera and/or a video camera. A computer was connected to the video and enabled numerical analyses to be performed.

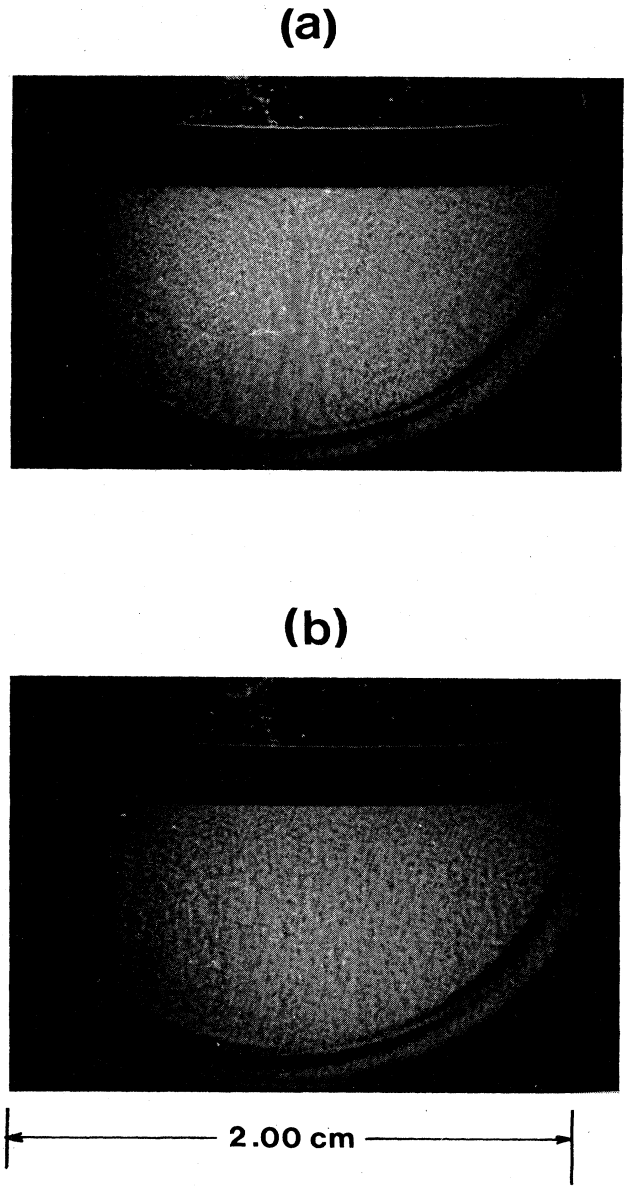

FIG. 14. Aspect of a 2-cm-diam sample of the C'-M mixture after a quench of 10 mK below T_c: (a); 1 min 15 sec after the quench: (b); 2 min after the quench. Note the presence of gravity-induced convections, to be compared with the structures observed in the Fig. 12.

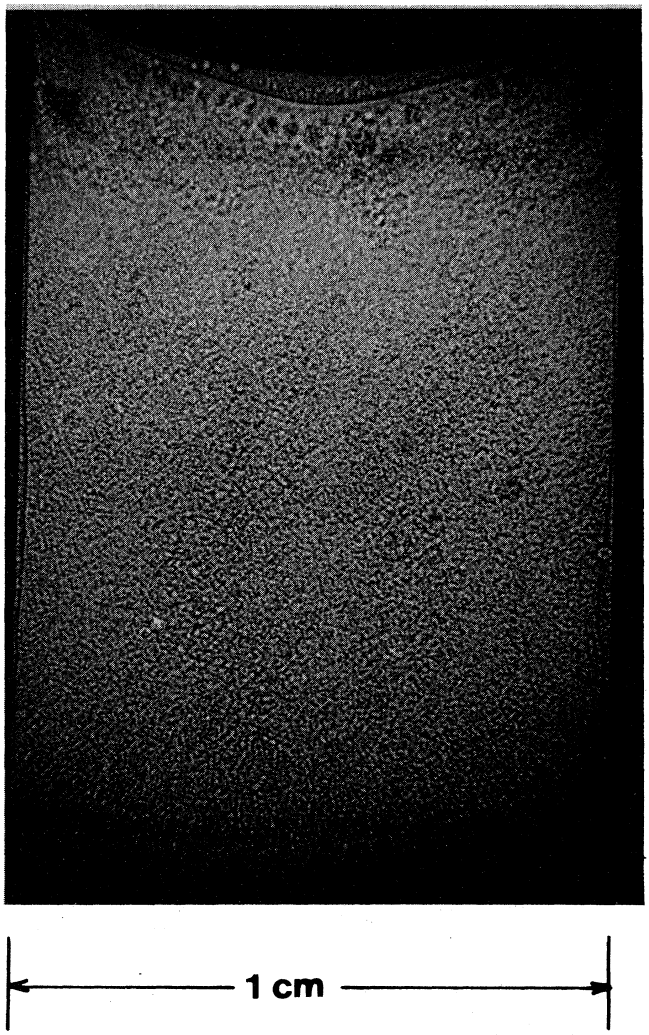

FIG. 15. Macroscopic wetting layers appearing 10 mK below T_c in the isopycnic $(C+C')$-M mixture, 16 min 50 sec after the quench.

C. Spinodal decomposition results

We report here the results of a typical quench where $T_i - T_c = 5$ mK and $T_f - T_c = -10$ mK. From a qualitative point of view one can distinguish two different stages as a function of the time θ after the quench:

(i) Classical SD process ($\theta < 1$ min; Fig. 10). Some seconds after the quench the well-known ring pattern appears in the scattered light. This ring collapses with time and after about 1 min becomes undetectable in the small angle stray light.

(ii) Macroscopic SD structures ($\theta > 1$ min; Fig. 12). The direct observation of the sample shows the presence of SD structures whose size increases slowly with time, from about 100 μm to reach the sample dimension (=1 cm) after 5 min.

In order to check the SD character of the structure we have performed a numerical two-dimensional Fourier transform; a well-defined ring was obtained (Fig. 13). We have also reported the structures shown by a nonisopycnic system, the C'-M mixture at the critical mass fraction $c = 0.731$. Figure 14, where raining structures are visible, shows that even for times $\theta \simeq 1$ min, convection occurs and that a meniscus becomes visible.

D. Wetting layers

In the stage (ii) of the above SD process, macroscopic wetting layers of the M-rich phase progressively form, showing droplets on the windows and irregular layers on the vapor interface and on the thin sides of the cell (Fig. 12). For longer times of the order of 15 min or more, well defined layers are formed (Fig. 15), whose shape depends on the cell shape.

Further from T_c ($T - T_c = -1$ K) the interfacial tension is large enough so that the mixture is formed of a drop of a $(C+C')$-rich phase surrounded by an M-rich phase wetting the walls and the meniscus with vapor (Fig. 16).

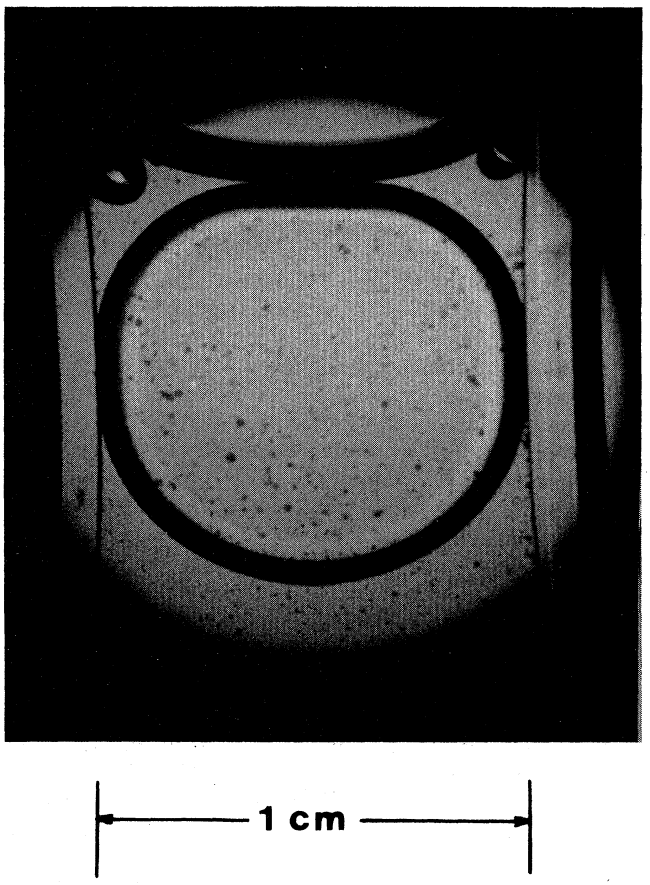

FIG. 16. Wetting layers appearing 1 K below T_c in the isopycnic $(C+C')$-M mixture.

It is clear that all the studies concerning the transitions between partial and complete wetting can be performed with macroscopic layers, to be compared with the 100 Å layer widths typically found in ordinary mixtures. Note that the mixture of acetonitrile and cyclohexane naturally exhibits closely matched densities, so that interesting wetting structures have been observed.[28] However, a supplementary degree of freedom is obtained with the $(C+C')$-M mixtures since the level of isodensity can be adjusted, in particular the $(C+C')$-rich phase can be made more dense or less dense according to the study or the temperature range of interest.

VII. CONCLUSION: PERSPECTIVES

The main conclusion of this study is that the ternary mixtures of cyclohexane, deuterated cyclohexane, and methanol behave as binary fluids with respect to the phase transitions properties. Moreover the critical amplitudes do not vary very much with respect to the C' concentration. The density of each phase can therefore be accurately adjusted so as to be matched; matching levels of about 10^{-6} g cm^{-3} have been obtained.

The applications of such a density matching can be numerous; in as much as that the gravity acts through the densities difference, valuable simulations of microgravity conditions can be performed. In particular the convections at constant temperature which appear at the phase transition of such binary fluids can be suppressed and new features appear: macroscopic periodiclike spinodal structures can be formed, whose size seems to be limited only by the sample size itself. The problem of the relevance of such finite size effects is now posed and could lead to interesting features. Also macroscopic wetting layers become visible, which makes the wetting phenomena easier to study. Note that the study of nucleation problems could be envisaged in terms of MG simulation.

However, the bulk of the sample is always submitted to ordinary gravity and thermal convections can appear under a temperature gradient. This could prevent any valid simulation of MG conditions, unless this thermal gradient is directed to have a stabilizing effect. In this case only Marangoni convections should occur, which could lead also to interesting effects.

ACKNOWLEDGMENTS

We gratefully acknowledge S. Tufeu for help in the measurements. This work was supported by grant from the Centre National d'Etudes Spatiales, France.

---

*To whom all correspondence should be sent.

[1](a) D. Beysens, in proceeding of the Fourth European Symposium on Materials Sciences under Microgravity, Madrid, 1983 [European Space Agency Report No. ESA-SP-191 (1983)]; (b) D. Beysens, in proceedings of the 35th Congress of the International Astronautical Federation, Lansanne, 1984 [Acta Astron. **12**, 141 (1985)].

[2]D. C. Jones and S. Amstell, J. Chem. Soc. 1316 (1930).

[3]E. L. Eckfeldt and W. W. Lucasse, J. Phys. Chem. **47**, 164 (1943).

[4]J. L. Tveekrem and D. T. Jacobs, Phys. Rev. A **27**, 2773 (1983).

[5]R. H. Cohn and D. T. Jacobs, J. Chem. Phys. **80**, 856 (1984).

[6]H. Wagenbreth and W. Blanke, *Internationalen Praktischen Temperaturskaler* (Springer, Berlin, 1968).

[7]Brunel and van Bib, *International Critical Tables* (McGraw-Hill, New York, 1928), Vol. 3, p. 27.

[8]*Handbook of Chemistry and Physics,* 44th ed. (Chemical Rubber, Cleveland, 1962).

[9]*Optische Konstanten,* Band 2, Teil 8 of *Landölt-Bornstein,* edited by K. H. Hellwege and A. M. Hellwege (Springer, Berlin, 1962).

[10]D. Beysens and P. Calmettes, J. Chem. Phys. **66**, 766 (1977).

[11]D. T. Jacobs, D. J. Anthony, R. C. Mockler, and W. J. O'Sullivan, Chem. Phys. **20**, 219 (1977).

[12]B. A. Scheibner, C. M. Sorensen, D. T. Jacobs, R. C. Mockler, and W. J. O'Sullivan, Chem. Phys. **31**, 209 (1978).

[13]M. Ley-Koo and M. S. Green, Phys. Rev. A **23**, 2650 (1981) and references therein.

[14]See, for instance, *Phase Transitions, Cargèse 1980,* edited by M. Lévy, J.-C. Le Guillou, and J. Zinn-Justin (Plenum, New York, 1982) and references therein.

[15]See, for instance, D. Beysens, J. Chem. Phys. **71**, 2557 (1979).

[16]V. Puglielli and N. Ford, Phys. Rev. Lett. **25**, 143 (1970).

[17]J. Yvon, *La Propagation et la Diffusion de la Lumière* (Hermann, Paris, 1937), p. 543; P. Calmettes, Opt. Commun. **44**, 306 (1983).

[18]M. F. Vuks, Opt. Spektrosk. **28**, 141 (1980) [Opt. Spectrosc. (USSR) **28**, 71 (1970)].

[19]See, for instance, D. Beysens, A. Bourgou, and P. Calmettes, Phys. Rev. A **26**, 3589 (1982), and references therein.

[20]R. B. Kopelman, R. W. Gammon and M. R. Moldover, Phys. Rev. A **29**, 2048 (1984), and references therein.

[21]D. Stauffer, M. Ferer, and M. Wortis, Phys. Rev. Lett. **29**, 345 (1972).

[22]P. C. Hohenberg, A. Aharony, B. I. Halperin, and E. D. Siggia, Phys. Rev. B **13**, 2986 (1976); C. Bagnuls, C. Bervillier and E. Boccara, Phys. Lett. **103A**, 411 (1984).

[23]B. Widom, J. Chem. Phys. **43**, 3892 (1965).

[24]Connie Warren and W. W. Webb, J. Chem. Phys. **50**, 3694 (1969).

[25]See, for instance, W. I. Goldburg, in *Scattering Techniques,* edited by S. H. Chen, B. Chu, and R. Nossal (Plenum, New York, 1981).

[26]J. W. Cahn, J. Chem. Phys. **42**, 93 (1965).

[27]F. B. Abraham, Phys. Rep. **53**, 93 (1979).

[28]V. Vani, S. Guha, E. S. R. Gopal, and S. Madhusudana Rao, Phys. Lett. **99A**, 441 (1983).

[29]C. M. Sorensen, R. Mockler, and W. O'Sullivan, Phys. Rev. A **16**, 365 (1977).

[30]Y. Yosida, Phys. Lett. A **65**, 161 (1977).

[31]M. A. Anisimov, A. V. Voronel, and T. M. Ovodova, Zh. Eksp. Teor. Fiz. **61**, 1092 (1971) [Sov. Phys.—JETP **34**, 583 (1972)].

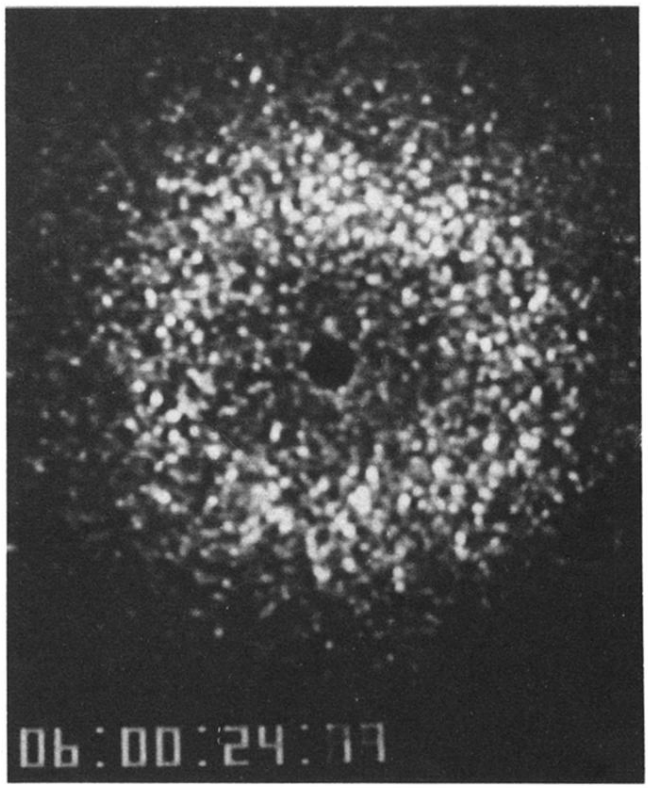

FIG. 10. Typical ring structure of the light scattered by a binary fluid undergoing spinodal decomposition. The corresponding wavelength is $\lambda_m \simeq 11$ μm (C'-M mixture, 24.77 sec after a thermal quench at $T_f - T_c = -1$ mK).

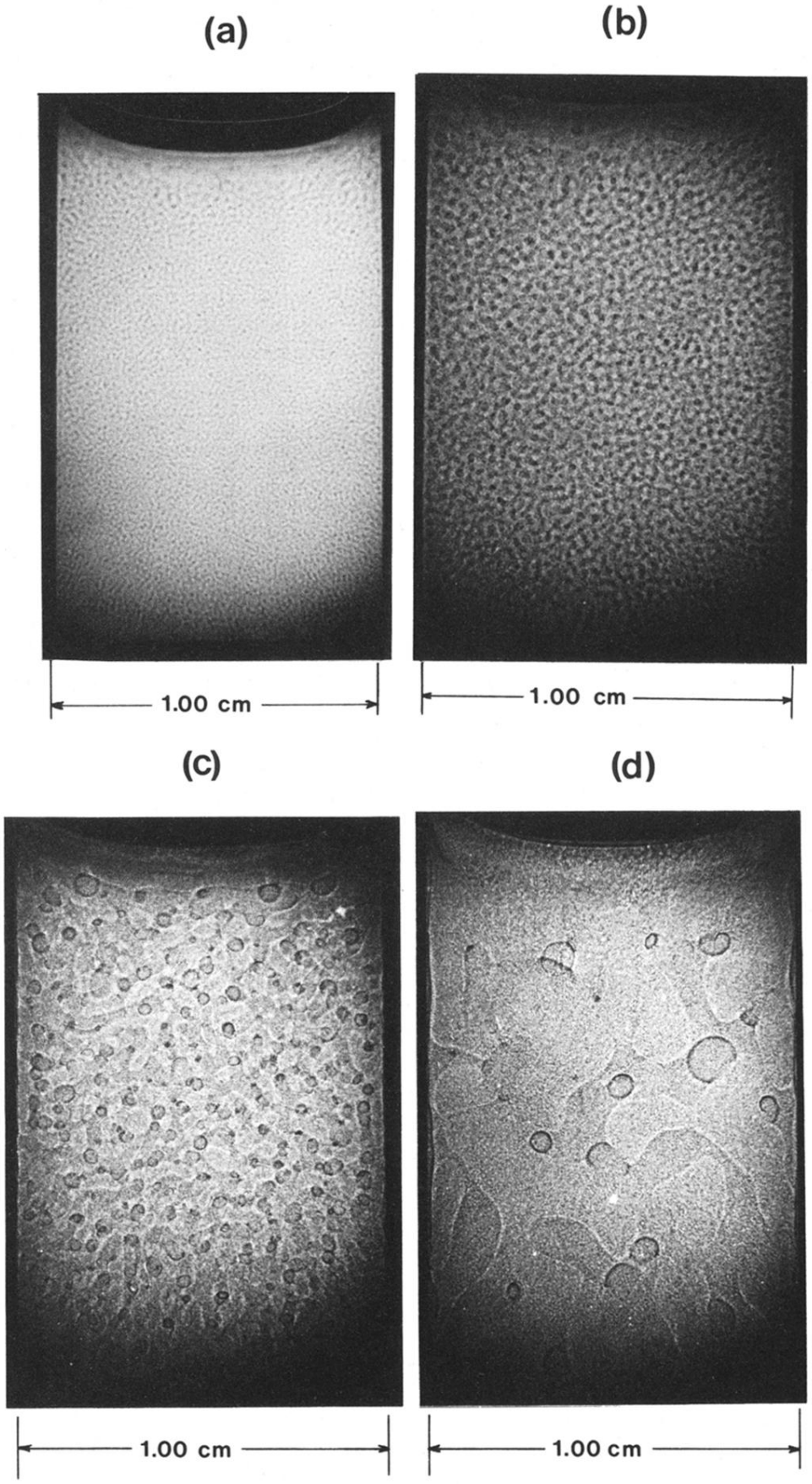

FIG. 12. Aspect of a 1×0.2-cm sample of the isopycnic $(C+C')$-M mixture after a quench of 10 mK below T_c. (a) 1 min 20 sec after the quench. (b) 2 min after the quench. (c) 4 min after the quench. (d) 9 min after the quench.

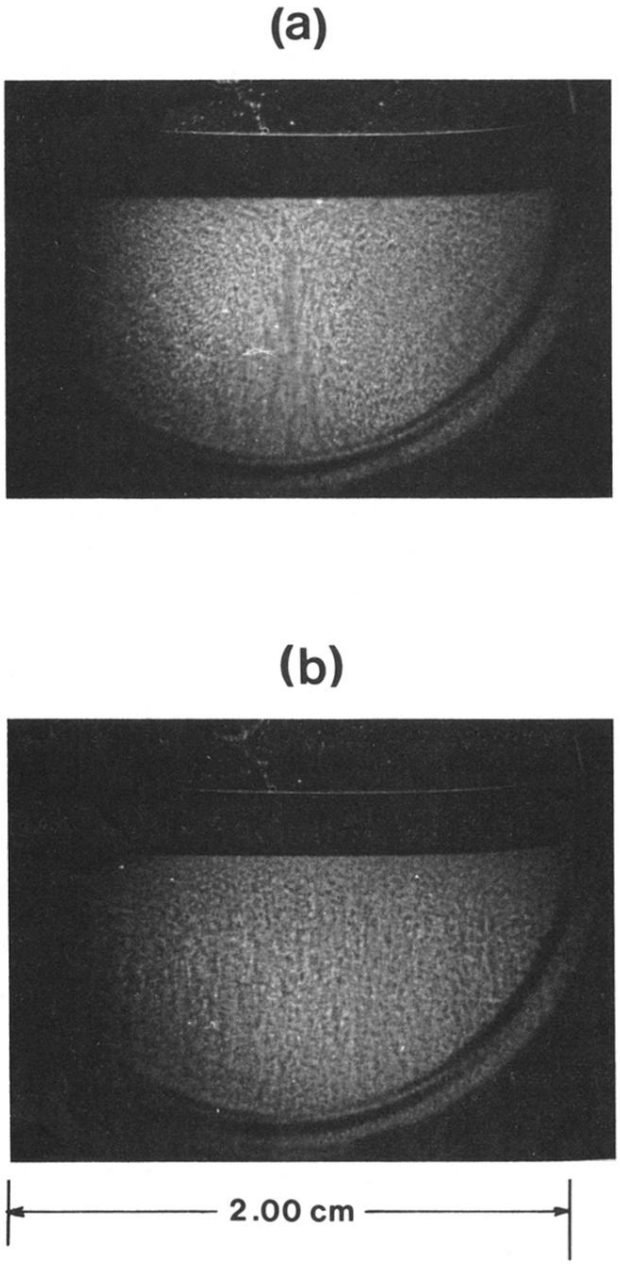

FIG. 14. Aspect of a 2-cm-diam sample of the C'-M mixture after a quench of 10 mK below T_c: (a); 1 min 15 sec after the quench: (b); 2 min after the quench. Note the presence of gravity-induced convections, to be compared with the structures observed in the Fig. 12.

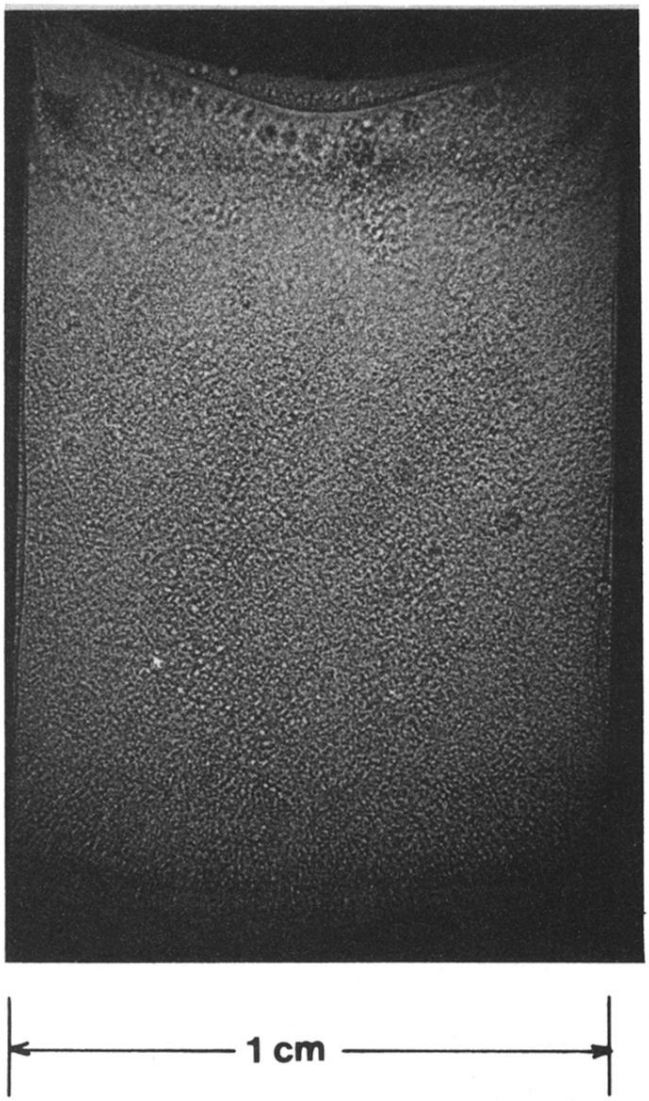

FIG. 15. Macroscopic wetting layers appearing 10 mK below T_c in the isopycnic $(C+C')$-M mixture, 16 min 50 sec after the quench.

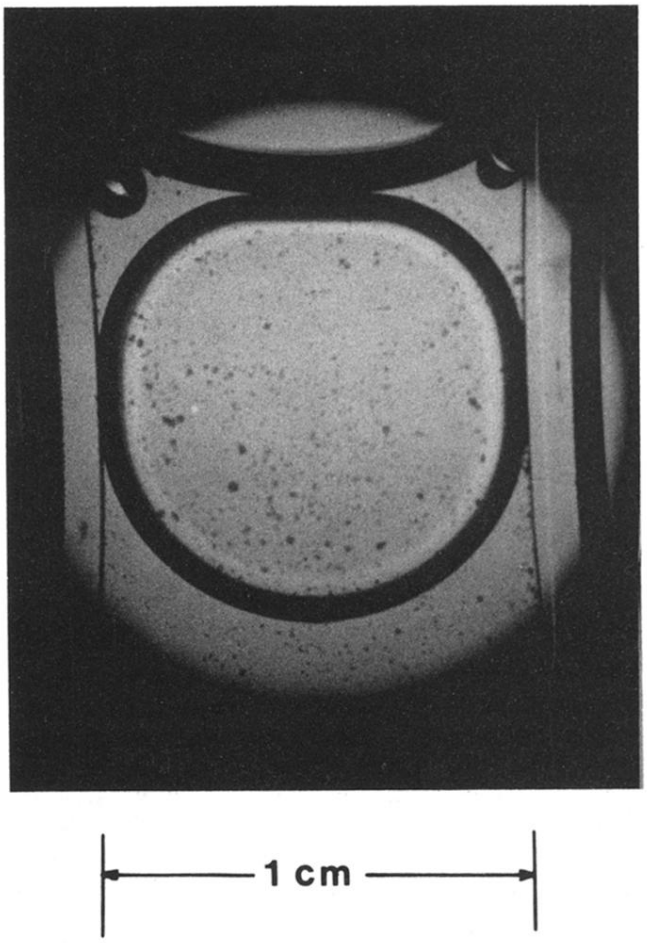

FIG. 16. Wetting layers appearing 1 K below T_c in the isopycnic $(C+C')$-M mixture.